Computational Urban Science

ORIGINAL PAPER

Open Access

Assessing UHI Impacts of Land Use Changes in Urban Development Areas through LCZ Classification

Muzeyyen Anil Senyel Kurkcuoglu[1*], Mehtap Ozenen-Kavlak[2,3], Halil Duymus[4] and Saye Nihan Cabuk[5]

Abstract

The study investigates the impact of the land use changes on the urban heat island effect ratio (UHIER), focusing on the urban development fringe of Ankara, Türkiye. Initially characterized by rural land uses the areas has experienced significant transformations into residential estates, mostly including high-rise blocks and low-rise villas. Urban development patterns in 2013 and 2023 were compared with changes in UHIER and local climate zone classes (LCZCs) using RS and GIS techniques for UHIER calculation, and the World Urban Database and Access Portal Tools (WUDAPT) protocol for LCZ mapping. Overall, UHIER values have a tendency to rise, as areas with increaing UHIER are found to be twice as large as those with decreasing UHIER. Increasing UHIER is highly associated with increases in open high-rise and sparsely built areas, accompanied by decreases in low plants. UHIER, on the other hand, is mosly characterized by a reduction in large low-rise built-types. The parts where UHIER remains unchanged suggests that although compact high-rise, open high-rise, and sparsely built areas have increased, the reduction in other built types—particularly large low-rise areas—along with a rise in tree density, appears to balance these changes. Therefore, to prevent high UHI impact when the area is fully developed, more landscaping features, particularly trees, can be integrated and mid-rise and low-rise developments can be preferred over high-rises, ensuring the efficient land use.

Keywords Urban heat island, Local climate zones, Land-use change, Urban development, GIS, RS

1 Introduction

Urban development has various environmental impacts due to the conversion of natural land cover into built-up areas, and effective land-use policies are required to control the negative externalities of the urban expansion, particularly to prevent the urban heat island (UHI) effect. The conversion of vegetated areas into impervious built-up surfaces is one of the most significant drivers of rising land surface temperatures, which contributes significantly to the formation of the UHI (Salam et al., 2024). Changes in urban land cover influence the city's thermal characteristics, including the UHI effect, and as land patterns shift, the landscape's ability to regulate the UHI also changes (Elliot et al., 2020). The increase in surface temperatures caused by higher densities, impervious surfaces, and surface albedo contributes

*Correspondence:
Muzeyyen Anil Senyel Kurkcuoglu
senyel@metu.edu.tr
[1] Department of City and Regional Planning, Faculty of Architecture, Middle East Technical University, 06800 Ankara, Türkiye
[2] Department of Geography, Faculty of Open and Distance Education, İstanbul University, 34398, Sarıyer, Istanbul, Türkiye
[3] Department of Remote Sensing and Geographical Information Systems, Institute of Earth and Space Sciences, Eskisehir Technical University, 26555 Eskişehir, Türkiye
[4] Department of Landscape Architecture, Faculty of Architecture, Çukurova University, Adana, Türkiye
[5] Institute of Earth and Space Sciences, Geodesy and Geographical Information Technologies Department, Eskisehir Technical University, Eskisehir 26555, Türkiye

© The Author(s) 2025. **Open Access** This article is licensed under a Creative Commons Attribution 4.0 International License, which permits use, sharing, adaptation, distribution and reproduction in any medium or format, as long as you give appropriate credit to the original author(s) and the source, provide a link to the Creative Commons licence, and indicate if changes were made. The images or other third party material in this article are included in the article's Creative Commons licence, unless indicated otherwise in a credit line to the material. If material is not included in the article's Creative Commons licence and your intended use is not permitted by statutory regulation or exceeds the permitted use, you will need to obtain permission directly from the copyright holder. To view a copy of this licence, visit http://creativecommons.org/licenses/by/4.0/.

to the UHI (Atasoy, 2020; Ding & Shi, 2013; Feng et al., 2014; Gee & Sarker, 2013; Hoan et al., 2018; Kamali Maskooni et al., 2021; Kim & Guldmann, 2014; Wang & Ouyang, 2017; Zhang et al., 2013; Zhou & Chen, 2018). Green spaces and vegetation, on the other hand, are effective solutions for mitigating and adapting to urban temperature conditions (Herath et al., 2018; Nastran et al., 2019; Ogce et al., 2025). Understanding the impacts of urban development and land use changes on the UHI and integrating this knowledge into urban planning efforts can improve the ability of cities to cope with climate change (Guindon & Nirupama, 2015; Ishibashi et al., 2019; Keith et al., 2023; Liang et al., 2021; MacLachlan et al., 2021; Onishi et al., 2010; Villanueva-Solis, 2017; Wang & Ouyang, 2017).

Remote sensing (RS) data and geographic information systems (GIS) techniques have been widely used to assess UHI impacts. These techniques offer practicality, cost advantages, and the advantage of time-series data availability (Tian et al., 2021). The impact of urban development on the UHI effect can be assessed by monitoring and analyzing land use/land cover (LULC) changes using RS and GIS techniques, which provide valuable insights for climate-responsive planning decisions. Local climate zone (LCZ) classificationd have been employed to assess LULC changes in urban development areas and to analyze their association with UHI variations over time. Acosta-Fernandez et al. (2025) mention the importance of LCZ classification in evaluating environmental impacts of urbanization, specifically in UHI mitigation. The LCZ scheme has rapidly gained acceptance across various disciplines for thermal characterization, integrating both urban and rural areas as part of the broader landscape, enabling clear characterization and comparison across different cities (Peiro et al., 2019).

While the UHI effect and LCZ have both been extensively studied, research combining these two approaches remains limited, particularly in the context of rapidly developing urban fringes in developing countries. Most studies focus on already urbanized cores or entire metropolitan regions (Lee et al., 2024; Rahmani & Sharifi, 2023; Wang et al., 2022; Dimitrov, 2021; Zhao et al., 2021; Yang et al., 2020; Leconte et al., 2015), overlooking peripheral development areas where urban growth is more dynamic and where planning interventions have the potential to mitigate future UHI impacts. Very few studies (Falah et al., 2024; Mushore et al., 2022; Zhang et al., 2021a, 2021b) explicitly address the UHI implications of newly developed areas transitioning from non-built-up to built-up land. In addition, studies focusing on urban development often highlight the impact of land-use functions associated with economic activities and production. Türkiye is one of the emerging economies facing rapid urbanization, of which urban population increased from 73% in 2013 to 78% in 2024**,** and projections indicate further growth (World Bank,(2025)). This rapid urbanization, if unmanaged, risks intensifying UHI effects and associated heat stress in cities, particularly in large metropolitan areas such as Ankara. The integration of UHI and LCZ provides a detailed understanding of how different built-up forms and green space configurations affect UHI formation in developing areas. This study considers the UHI impacts of urban development areas primarily in the context of residential developments, based on LCZ changes and offers planning-relevant insights for sustainable urbanization strategies in developing countries**,** contributing both to academic discourse and practical policy-making. The UHI impact is assessed through the Urban Heat Island Effect Ratio (UHIER) for Ankara, Türkiye, over the period 2013–2023. RS and GIS techniques are utilized to generate UHIER maps, while an open community-based modelling platform, World Urban Database and Access Portal Tools (WUDAPT), is employed for LCZ mapping of various built-up and land cover types.

2 Literature Review

Several studies have highlighted how urbanization and LULC changes influence urban thermal conditions in terms of UHI effect (Hu & Jia, 2010; Tang et al., 2017; Zhang et al., 2021a, 2021b). The use of RS and GIS techniques stands out by providing cost and time efficiency, and by enabling repeatable, practical, and timely analyses in addressing such issues. For instance, Zhou and Chen (2018) observed that LULC changes between 1965 and 2008 intensified the UHI effect in Wuhan, China. Similarly, Zhao et al. (2016) found that rapid urban expansion in Shanghai between 1984 and 2014, particularly in areas with wide roads and compact low-rise buildins, significantly exacerbated the UHI effect. In the Pearl River Delta, China, Chen et al. (2006) employed RS to show that UHI intensity was particularly pronounced in rapidly urbanizing areas between 1990 and 2000. In studies employing RS data, thermal imagery from satellite sources such as Landsat and MODIS has been widely utilized to derive land surface temperature (LST) data and assess the spatial and temporal dynamics of the UHI phenomenon (Aik et al., 2020; Liu et al., 2016; Shi et al., 2021; Weng et al., 2014). Li and Yin (2013) used Landsat and MODIS data to examine the spatial and temporal dynamics of UHI in Shanghai from 1995 to 2012, observing a shift from a citywide UHIER pattern to one concentrated around urban cores and other built-up zones as a result of urban expansion.

The literature emphasizes not only the impact of LULC on UHI formation but also the role of land-use strategies, such as the implementation of green infrastructure, in mitigating UHI effects in high-density urban areas (Sharifi & Lehmann, 2014). Comprehensive reviews by Rizwan et al. (2008) and Kardinal Jusuf et al. (2007) highlight the critical role of urban design and planning in mitigating UHI impacts, while Ananyeva and Emmanuel (2023) further demonstrate that vegetation can substantially reduce surface temperatures, particularly in densely built environments. In Brazil, Nakata-Osaki et al. (2018) developed a GIS-based model by adapting an empirical formulation originally designed to estimate nocturnal UHI intensity based on urban geometry. By integrating urban morphology within a GIS framework, their model improved the prediction of UHI intensity in Brazilian cities. Many of these studies apply quantitative methods, utilizing various indices to examine the relationship between surface temperature and land cover characteristics. Certain other studies employ simulation approaches, integrating machine learning and RS data, to forecast future UHI trends and impacts, highlighting the interconnectedness between urbanization, climate change, and environmental challenges such as increased heat stress and heat vulnerability (Garzon et al., 2021; Liu et al., 2021, 2024; Lyu et al., 2022; Li et al., 2024).

Recently, the LCZ classification has been increasingly integrated into urban climate studies, offering a standardized framework to distinguish urban and rural thermal environments based on surface cover and urban geometry. This approach enables more detailed assessments of the UHI effect by capturing variations in urban forms and land use (Stewart & Oke, 2012; Zhao et al., 2019). The LCZ scheme has been instrumental in UHI analysis across diverse contexts. Numerous studies have demonstrated that LCZ types exhibit distinct thermal behaviors: compact or high-density built-up zones generally produce stronger UHI effects than open or natural environments (Chen et al., 2023; Yang et al., 2020). Similarly, Wu et al. (2025) revealed that LCZ types associated with natural land cover mitigate SUHI, whereas built-up types tend to increase LST and, consequently, SUHI. LCZ-based methods have been widely applied in both comparative and site-specific studies. For instance, Bechtel et al. (2019) examined SUHI patterns across 50 cities using MODIS and Landsat 8 data within the WUDAPT framework, while Lee et al. (2024) linked planning-related LCZ variations in South Korea to differences in SUHI intensity and heat vulnerability. Applications have also extended to complex terrains and microclimate studies. Badaro-Saliba et al. (2021) investigated LST–LCZ relationships in the mountainous areas of Beirut, while Lau et al. (2019) combined objective thermal data with subjective heat perceptions across eight LCZs in Hong Kong, identifying significantly warmer sensations in compact high-rise areas. Parvar et al. (2024) highlighted the cooling benefits of increasing vegetation cover in relation to building density and height, and Rahmani and Sharifi (2025) emphasized that inefficient layouts, high density, and insufficient vegetation exacerbate UHI effects, whereas green spaces mitigate heat stress. Consistently, Shi et al. (2022) showed that constructed LCZs, particularly heavy industrial zones, exhibit the highest UHI indices, while natural LCZs such as ventilated corridors and scattered tree areas provide notable cooling effects.

Building on this growing body of LCZ-based research, several case studies have further demonstrated how the expansion and spatial arrangement of LCZs influence UHI intensity and its spatial variability. Mushore et al. (2022) used the WUDAPT protocol to map LCZs in Bulawayo, Zimbabwe, and revealed that the expansion of built-up LCZs led to an increase in urban heat island (UHI) intensity, while deforestation and the expansion of lightweight low-rise, as well as compact and open low-rise zones, contributed to higher surface temperatures. Similarly, Rahmani and Sharifi (2023) adopted the WUDAPT protocol to provide LCZ classifications for two Japanese cities, Sapporo and Hiroshima, and utilized Landsat 7 and 8 data to retrieve temporal LCZs. Their study indicated that LCZs with minimal green cover—such as heavy industry, large low-rise, bare rock and paved surfaces, and compact low-rise—tended to deteriorate thermal comfort, and that areas with warmer climates and denser urban development were more susceptible to SUHI effects. Zhang et al., (2021a, 2021b) found that land cover type and surface structure significantly influenced local climate, and that UHI magnitude varied notably across LCZ types. Their findings showed that the highest UHI occurred in the large low-rise LCZ group, while compact mid-rise and compact low-rise zones also exhibited elevated UHI, in contrast to newly developed areas with substantial greening and a few open high-rise residential or commercial buildings, where UHI was lower. Falah et al. (2024) examined the thermal impact of urbanization on LCZs and LST in Seville, Spain, where built-up areas increased approximately 1.5 times and urban development shifted from compact to more dispersed and ribbon patterns, particularly in the outskirts. LCZs such as dense trees and scattered trees, along with urban greening policies, were found to slightly mitigate temperature increases in some areas. Dimitrov et al. (2021) conducted a thermal survey of Sofia, Bulgaria, in August 2019, and reported that the highest surface temperatures occurred in sparsely built, open high-rise, and open mid-rise LCZs, whereas low-plant

and bush and scrub areas represented the coolest zones. Wu et al. (2022) investigated thermal comfort in different urban environment in terms of LCZs in Shenzen, China using the data of 65 weather stations for the year 2020. They concluded thermal comfort patterns vary across various LCZ types.

In this study, the LCZ approach developed by Stewart and Oke (2012) is adopted to evaluate the local-scale impacts of different built-up types and densities, as well as open green space uses, on the UHI effect in urban development areas. The WUDAPT protocol, as an open-source tool, is utilized to evaluate the impact of specified LULC types through LCZ mapping of the south-western urban development zone of Ankara over a decade. In this way, the UHI effects of different urban fabrics and land use patterns in a still-developing area will be revealed, contributing to the literature. The impact of variations in urban density and spatial patterns on the urban heat island effect will also provide guidance for future planning studies from the perspectives of sustainability and livability. Although numerous studies have analyzed the UHI effect and adopted the LCZ framework in various contexts, the combined application of LCZ and UHI metrics in rapidly developing urban fringe areas are overlooked. Most of the previous research has focused on well-established urban cores or entire metropolitan regions, leaving a gap in understanding thermal implications in new development zones transitioning from non-built-up to built-up land. This study addresses that gap by integrating UHIER analysis with LCZ classification over a decade in Ankara's southwestern development corridor, a representative case of rapid urban growth in a developing country context. By linking spatially explicit LCZ transitions to pixel-level UHIER changes, this research provides empirical evidence on how specific development patterns, primarily in the context of residential land-uses, intensify or mitigate urban heat, offering both theoretical contributions to urban climate literature and practical insights for climate-sensitive planning in emerging economies.

3 Methodology

This section gives information about this study area, data, and methods used. First the study area is introduced. Then, UHIER calculations and LCZ analysis are discussed.

3.1 Study Area

The study area is located in the southwestern part of Ankara, the capital of Türkiye. Ankara has a dry-summer continental climate, a subtype of the temperate climate, characterized by hot and arid summers, cold winters, and pronounced seasonal temperature variations. Kong et al. (2025) stated that cities located in temperate climates tend to experience stronger UHI effects compared to those in tropical climates. The population of Ankara has exhibited a steady increase, growing from 5,045,083 in 2013 to 5,803,482 in 2023 (TUIK, 2025). The city has a dynamic character in terms of successive land use changes, driven by population growth through urban fringe expansion and urban regeneration activities in built-up areas. Demographic changes have intensified the demand for housing and other urban services, leading to rapid urban development. However, the extent to which this development aligns with the principles of sustainability and livability, one of which is the UHI effect, remains unclear. Considering these factors, the study area was selected from one of the fastest-developing urban zones on the southwestern fringe of the city, encompassing recent built-up developments in the Kızılcasar, İncek, Dodurga, and Alacaatlı neighborhoods (Fig. 1). To effectively capture the UHI effect, the study focused exclusively on the rapidly developing urban fringe, which exhibits concentrated new built-up areas. For this reason, the study area has an irregular shape, reflecting the spatial pattern of recent urban growth.

The area has been predominantly transformed in the past decade by high-rise point blocks and low-rise villa settlements, replacing many other land uses — particularly rural ones. Urban development in the area has expanded spatially, and the real estate market gained significance between 2010 and 2020, while the southwestern urban fringe of Ankara emerged as a high-demand zone that experienced a rapid urbanization process over this period. It can be stated that planning had a primary influence on location selection during the planning periods and on the densification of settlements between 2010 and 2020 (Güneş, 2021). Dağlıoğlu (2024) notes that the area has significant potential as a basis for understanding the city's primary growth and expansion dynamics and that it has undergone rapid transformation driven by land speculation over the past two decades. She further argues that the area hosted a few small rural settlements and a limited number of low-density gated communities before the early 2000s, whereas following the construction of two high-rise residential complexes in 2012, numerous new buildings were added, accelerating the urbanization of the surrounding area. The most significant changes in UHIER are anticipated to occur in these development areas, where rural land uses — primarily dominated by natural land cover — are being replaced by urban land uses characterized by built structures and impervious surfaces.

3.2 Data

This study utilized RS data and data generated through the WUDAPT platform. Landsat 8 satellite

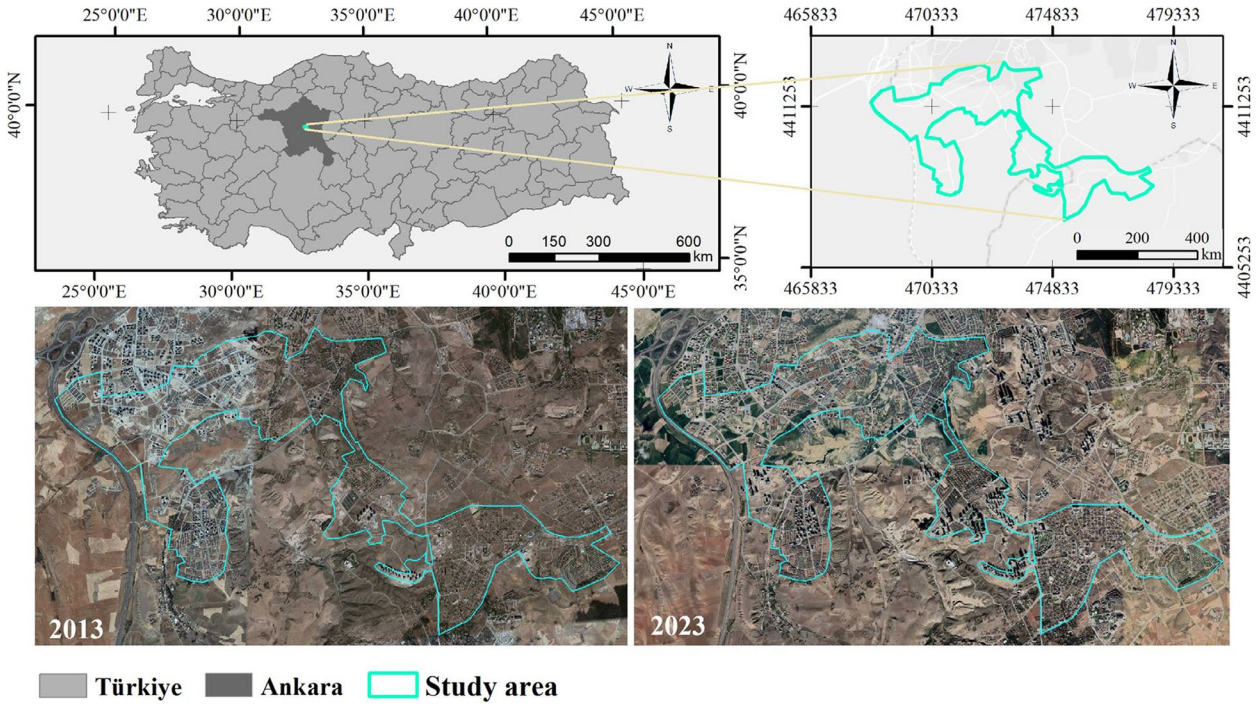


Fig. 1 Study area

imagery for the summer seasons of 2013 and 2023 was obtained from the USGS platform. Scenes with cloud-free conditions over the study area were selected to ensure the consistency and reliability of the analysis. The reference years, 2013 and 2023, were selected to capture the long-term impact of urban development on UHIER. 2013 marks the earliest period with consistent Landsat 8 data and stable LCZ classification, while 2023 represents the most recent year with cloud-free summer scenes, reflecting peak UHI conditions. Table 1 provides details about the technical specifications. Although the thermal band has an original image resolution of 100 m, it is resampled to 30 m by the data provider before being made available to users.

The images were processed using ArcGIS 10.8.2 software, applying established formulas from the literature to determine the UHIER value for the region. The study area boundaries were acquired in vector data format, and statistical analyses were conducted using Microsoft Excel.

In order to compare 2013 and 2023 summer temperatures, 92 daily temperature records were included in the analysis covering daily records of June, July and August, retrieved from an open source (AccuWeather.com) which retrieves its records from the Esenboğa Airport weather monitoring station—the only consistently available station in Ankara throughout the full study period. A one-way analysis of variance (ANOVA) was performed to evaluate the difference in summer temperatures between 2013 and 2023. Although the results indicated a statistically significant difference between the two years, $F(1, 182) = 8.25$, $p = .0046$, the effect size, calculated using Cohen's d, was 0.42, indicating a small to medium effect. The mean average summer temperature in 2013 was

Table 1 The information about satellite images used in the study

Date of image capturing	Name of the satellite	Bands used in the study	Wavelength (micrometers)	Resolution (meters)
23.06.2013	Landsat 8			
25.07.2013				
10.08.2013		Band 4—Red	0.64–0.67	30
27.06.2023		Band 5—Near Infrared (NIR)	0.85–0.88	30
21.07.2023		Band 10—Thermal Infrared (TIRS) 1	10.6–11.19	100 (30)
06.08.2023				

21.30 °C, while in 2023 it was 22.71 °C. These findings suggest that while 2023 was warmer than 2013, the difference falls within a moderate range and does not reflect an extreme thermal anomaly. Therefore, the selected satellite scenes can be considered representative of typical summer conditions in their respective years. This supports the temporal validity of the imagery and addresses concerns about potential bias introduced by using a limited number of scenes per year.

The data used in the LCZ analysis were generated through WUDAPT, an international community-based modeling framework that produces and disseminates climate-responsive urban data (Ching et al., 2018). Training areas are created for 2013 and 2023 as instructed in WUDAPT, which include 17 climate zones classes (Demuzere et al., 2021). These classes comprise 10 built types and 7 land cover types, based on the classification by Stewart and Oke (2012), as presented in Table 2. It should be noted that LCZ classifications include information on building materials, building height, and density, all of which are considered factors affecting surface temperature variations.

Various representative areas for each group are selected within approximately 32,000 hectares throughout Ankara, covering both the built-up and rural areas. Then, the training areas are loaded to LCZ generator in WUDAPT webpage and the resulting LCZ map along with data files, factsheets, and figures are obtained. The overall accuracy (OA) turns out to be higher for the most recent year, 2023, compared to the previous period, 2013, with values of 0.81 and 0.72, respectively. The lower accuracy of the previous period can be attributed to the prevalence of squatter settlements, since the outputs show that the lowest accuracy belongs to LCZ class 3, compact low-rise. The classification of these irregular settlements has posed challenges due to the small size of individual buildings, which often led to their misclassification as land cover types such as bush or scrub. Furthermore, many of

Table 2 LCZ Classes with definitions (Stewart & Oke, 2012)

LCZ Code		Name	Definition
Built types	1	compact high-rise	Dense mix of tall buildings to tens of stories. Few or no trees. Land cover mostly paved. Concrete, steel, stone, and glass construction materials.
	2	compact mid-rise	Dense mix of midrise buildings (3–9 stories). Few or no trees. Land cover mostly paved. Stone, brick, tile, and concrete construction materials
	3	compact low-rise	Dense mix of low-rise buildings (1–3 stories). Few or no trees. Land cover mostly paved. Stone, brick, tile, and concrete construction materials
	4	open high-rise	Open arrangement of tall buildings to tens of stories. Abundance of pervious land cover (low plants, scattered trees). Concrete, steel, stone, and glass construction materials
	5	open mid-rise	Open arrangement of midrise buildings (3–9 stories). Abundance of pervious land cover (low plants, scattered trees). Concrete, steel, stone, and glass construction materials
	6	open low-rise	Open arrangement of low-rise buildings (1–3 stories). Abundance of pervious land cover (low plants, scattered trees). Wood, brick, stone, tile, and concrete construction materials
	7	lightweight low-rise	Dense mix of single-story buildings. Few or no trees. Land cover mostly hard-packed. Lightweight construction materials (e.g., wood, thatch, corrugated metal)
	8	large low-rise	Open arrangement of large low-rise buildings (1–3 stories). Few or no trees. Land cover mostly paved. Steel, concrete, metal, and stone construction materials
	9	sparsely built	Sparse arrangement of small or medium-sized buildings in a natural setting. Abundance of pervious land cover (low plants, scattered trees)
	10	heavy industry	Low-rise and midrise industrial structures (towers, tanks, stacks). Few or no trees. Land cover mostly paved or hard-packed. Metal, steel, and concrete construction materials
Land cover types	A	dense trees	Heavily wooded landscape of deciduous and/or evergreen trees. Land cover mostly pervious (low plants). Zone function is natural forest, tree cultivation, or urban park
	B	scattered trees	Lightly wooded landscape of deciduous and/or evergreen trees Land cover mostly pervious (low plants). Zone function is natural forest, tree cultivation, or urban park
	C	bush, scrub	Open arrangement of bushes, shrubs, and short, woody trees. Land cover mostly pervious (bare soil or sand). Zone function is natural scrubland or agriculture
	D	low plants	Featureless landscape of grass or herbaceous plants/crops. Few or no trees. Zone function is natural grassland, agriculture, or urban park
	E	bare rock or paved	Featureless landscape of rock or paved cover. Few or no trees or plants. Zone function is natural desert (rock) or urban transportation
	F	bare soil or sand	Featureless landscape of soil or sand cover. Few or no trees or plants. Zone function is natural desert or agriculture
	G	water	Large, open water bodies such as seas and lakes, or small bodies such as rivers, reservoirs, and lagoons

these settlements were situated in topographically disadvantaged areas, such as steep slopes, making it difficult to distinguish their density as either open or compact. By 2023, however, most of these areas—particularly those on steep terrain—have either been removed or transformed as a result of intensive urban regeneration efforts over the past decade.

At this point, it is important to note that the accuracy assessment was conducted for the entire Ankara metropolitan area, including its surrounding rural regions, covering approximately 32,000 hectares. In contrast, the study area is limited to the southwestern development corridor, accounting for approximately 5% of the total region of interest. Moreover, irregular settlements have not been observed in this area—neither in the past nor in recent years—as it is a designated planned development zone of Ankara.

When the accuracy assessment was conducted exclusively for the study area, the results showed a substantial improvement. Considering the likelihood that a given pixel belongs to a specific LCZ class for the study area, it is observed that in the 2013 LCZ map, 90% of the area has a probability of 50% or higher, and 71% of the area has a probability of 70% or higher. Class probabilities for 2023 are considerably higher, with 92% of the area having a probability of 50% or higher, 83% of the area having a probability of 70% or higher, and 74% of the area having a probability of 90% or higher (Fig. 2). As higher probabilities indicate greater confidence in the classification and increase the reliability of the LCZ map, the over-mentioned probabilities are considered acceptable in data accuracy of the study area.

To assess sensitivity, we examined the proportion of low-confidence areas with less than 50% probability (Table 3). These accounted for around 10% of the study area in 2013 and 8% in 2023, indicating that low-confidence zones have limited spatial influence on the overall findings. The probability-based accuracy assessment indicates that the majority of LCZ-classified pixels have a high level of confidence implying that misclassifications are spatially limited and unlikely to influence the interpretation of UHIER patterns at the study area, demonstrated in Fig. 2.

Table 3 Probability-Based Accuracy Metrics for LCZ Classifications

Metric	2013	2023
Weighted Mean Prob	0.813	0.846
Weighted Std Dev	0.194	0.191
% Pixels ≥ 50%	90	92

3.3 Method

The primary method employed in the study involves the analysis of satellite imagery and statistical evaluation within a GIS environment. The generated UHIER changes are compared to the changes in LCZ classes in the study area, in order to reveal the impact of the change in land use types in UHI values. The method covers four main steps: (1) Extraction of the satellite images (2) UHIER calculation, (3) LCZ mapping, and (4) Comparison of the changes in UHIER and LCZ classes (Fig. 3).

3.4 UHIER calculation

The UHI effect suggests that land surface temperatures are higher in urban areas influenced by anthropogenic development compared to rural areas (Oke, 1973; Tsou et al., 2017). This impact is primarily driven by LULC changes and urbanization (Du et al., 2020; Estoque et al.,

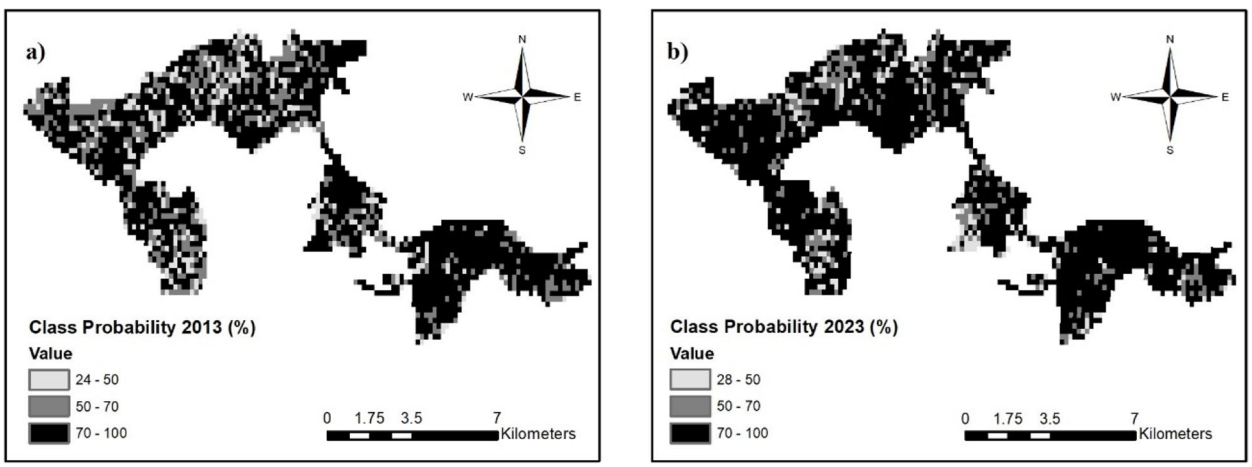


Fig. 2 Spatial distribution of class probabilities in generated LCZ maps for 2013 (**a**) and 2023 (**b**)

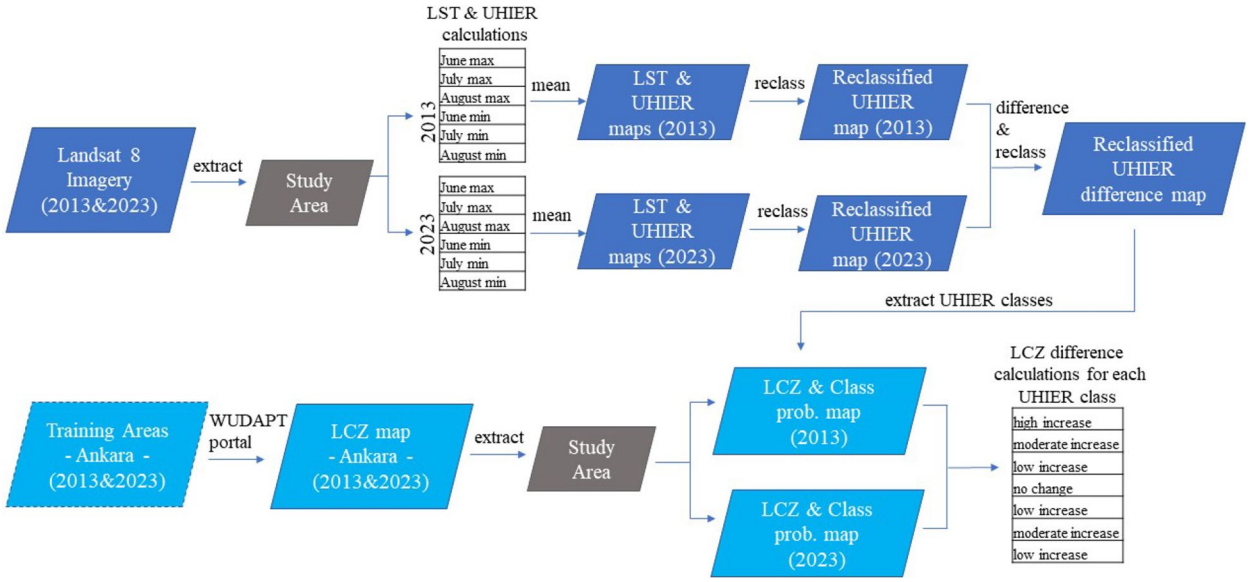


Fig. 3 Flowchart for the methodology of the study

2017; Zhao et al., 2014). The intensity of the temperature difference between urban and rural areas can be measured by calculating the UHIER (Portela et al., 2020).

RS methods (Cetin et al., 2024; Li & Yin, 2013; Li et al., 2014; Pan, 2016) and Landsat satellite images with thermal bands are frequently used in UHI calculations (Halder et al., 2022; Hasanlou & Mostofi, 2015; Seletković et al., 2023; Sheng et al., 2017). Landsat's provision of free, open-access data, along with its long-term, uninterrupted observation program, makes it particularly suitable for temporal studies of the same location. The steps necessary to calculate UHIER using RS methods are outlined in Table 4.

According to the applied approaches and formulas, UHIER results are categorized based on their intensity levels (Table 5) (Huang et al., 2019; Zhang et al., 2013). In this study, UHIER values were assessed at four different levels, ranging from moderately cooler to moderately warmer. The UHIER result map categorizes the minimum and maximum values into two classes, with"0"at the center, representing the dividing point between negative and positive values. A negative UHIER result indicates that rural areas are warmer than urban areas, while a positive UHIER result indicates that rural areas are cooler than urban areas. As values approach zero, it suggests a decreasing temperature difference between urban and rural areas. The UHI maps generated from the study area were reclassified according to the categories in Table 5. This reclassification enabled the calculation of areas exhibiting increases or decreases in UHI values, both in spatial extent and percentage terms.

To generate the UHIER map, LST and corresponding rural LST maps were first produced separately for June, July, and August in both 2013 and 2023. This process yielded a total of six LST and corresponding UHIER maps, calculated using the formula presented in Table 4. For each year, the three monthly LST and UHIER maps were averaged in a GIS environment to produce composite LST and UHIER maps representing 2013 and 2023, respectively. To analyze temporal changes, pixel-wise difference maps were generated using map algebra by subtracting the 2013 UHIER values from the 2023 map. Furthermore, the same method was applied to the reclassified UHIER maps, resulting in both original and reclassified UHIER difference maps.

In the reclassified UHIER difference maps, identifying specific category transitions—such as a shift from a moderately cooler class in 2013 to a moderately warmer class in 2023—is essential for understanding the spatial dynamics of UHIER change. To achieve this, a total of 18,777 points, each corresponding to a single pixel (30 m x 30 m), were systematically distributed across the reclassified UHIER maps for both years. The UHIER class values at these point locations were extracted using a GIS environment.

3.5 LCZ Mapping

LCZC scheme, derived from Stewart and Oke, provides a standardized categorization of land according to built and land cover types with regard to surface characteristics, material, structure, and human activity (Stewart & Oke, 2012). The classification considers height of the

Table 4 Analyses and formula for Landsat 8 (Cetin et al., 2022; Huang et al., 2019; Kumar et al., 2022)

Analysis	Formula	Definitions
Normalized Difference Vegetation Index (NDVI)	$(NIR - RED)/(NIR + RED)$	• NIR = 5th band (Landsat 8) • RED = 4th band (Landsat 8)
Top of atmospheric reflectance (TOA)	$ML * Qcal + AL$	• ML = Radiance multiplicative Band (No.10) • AL = Radiance Add Band (No.10) • Qcal = Quantized and calibrated standard product pixel values (DN)
TOA to brightness temperature (BT) conversion	$(K_2/(\ln(K1/L) + 1)) - 273.15$	• K_1 = Band-specific thermal conversion was constant from the metadata (774.8853) • K_2 = Band-specific thermal conversion was constant from the metadata (1321.0789) • L = TOA • To obtain the results in Celsius, the radiant temperature is adjusted by adding the absolute zero (approx. – 273.15 °C)
Proportion of vegetation (P_V)	$((NDVI - NDVI_{min})/(NDVI_{max} - NDVI_{min}))^2$	• The minimum and maximum values of the NDVI image can be displayed directly in the image
Land surface emissivity (ε)	$0.004 * Pv + 0.986$	• Pv = Proportion of vegetation • The value of 0.986 corresponds to a correction value of the Equation
LST	$(BT/(1 + (\lambda * BT/C2) * Ln(\varepsilon)))$ $(BT/(1 + (0.00115 * BT/1.4388) * Ln(\varepsilon)))$	• BT = Top of atmosphere brightness temperature (°C) • λ = Wavelength of emitted radiance (0.00115) • C2 = h*c/s = 1.4388 × 10–2 mK = 14,388 mK h = Planck's constant = 6.626 × 10–34 J s s = Boltzmann constant = 1.38 × 10–23 JK c = Velocity of light = 2.998 × 108 m/s • ε = Land surface emissivity
UHIER	ΔTi/Ts = (Ti-Ts)/Ts	• Ti = The LST of the i-th pixel • Ts = The mean LST of rural lands

Table 5 UHIER Intensity categories, value ranges, and thermal interpretation

UHIER Value	Level	Explanation
[–0.17] – [–0.085]	Moderately cooler	LST value in the urban area is moderately cooler than the rural area
[–0.085] – [0]	Slightly cooler	LST value in the urban area is slightly cooler than the rural area
[0] – [0.085]	Slightly warmer	LST value in the urban area is slightly warmer than the rural area
[0.085] – [0.17]	Moderately warmer	LST value in the urban area is moderately warmer than the rural area

buildings and surface material, as well as construction material and densities in built types. For rural areas, land cover type that dominates the area defines the LCZ class.

In this study, WUDAPT protocol is adopted for LCZ mapping of Ankara for the respective years. As outlined by Demuzere et al. (2021), the WUDAPT protocol facilitates the creation of LCZ maps and provides a framework for evaluating their classification accuracy. The protocol works with Google Earth Engine in creating training areas for a single city for a given time. Then, the training areas are uploaded to the WUDAPT portal to generate a LCZ map fort the whole city and its surroundings. The resulting output includes the generated LCZ map along with the associated data files, factsheets, and figures, reporting the overall accuracy (OA), the overall accuracy for urban LCZ classes (OAu), the overall accuracy for built versus natural LCZ classes (OAbu), and the weighted overall accuracy (OAw). (Demuzere et al., 2021). The accuracies are discussed in the data section in detail, where it is stated that for the year 2013, 71% of the study area, and for 2023, 83% of the study area, achieved a classification accuracy above 70%, indicating a high level of consistency in classification within the study area boundaries.

3.6 Comparison of UHIER and LCZ classes

In the third stage of the analysis, changes from 2013 to 2023 were examined by comparing UHIER and LCZ differences. LCZ values for 2013 and 2023 are calculated for the areas in 6 UHIER difference groups – high decrease, moderate decrease, low decrease, no change, low increase, moderate increase, and high increase – by extracting LCZ classes from each UHIER difference group through raster extraction. The resulting LCZ

difference between 2013 and 2023 is also standardized to reveal the most significant area increase/decrease in each LCZ class.

A statistical analysis is provided to understand whether the variation of UHIER among LCZ groups is significant. The data for LCZ values are nominal, thus, a non-parametric Kruskal Wallis test is utilized to compare the groups, and the null hypothesis states that the mean ranks are the same in all groups.

$$H = \frac{12}{N(N+1)} \sum_{i=1}^{k} \frac{R_i^2}{n_i} - 3(N+1)$$

where H is the Kruskal Wallis H Statistics.

N is the total number of observations.

n_i is the number of observations in group i,

R_i is the sum of the ranks in group i.

At this point, it is important to clarify that UHIER maps are generated at a 30 m × 30 m resolution using the WGS 1984 UTM Zone 36 N projection, whereas LCZ maps are originally in an unprojected coordinate system. When LCZ maps are reprojected to WGS 1984 UTM Zone 36 N, their resolution defaults to approximately 87.88 m × 87.88 m. As a result, some degree of misalignment may occur when overlaying the two raster datasets; however, this discrepancy is considered negligible for the purposes of this study.

4 Results

In this part of the study, results of LST, UHIER and LCZ analyses are demonstrated.

4.1 LST and UHIER Results

LST and UHIER values were calculated based on monthly maximum and minimum temperatures, as well as mean rural LST values, and the results are presented in Table 6.

The LST maps for June, July, and August of 2013 and 2023 were produced and presented in Fig. 4(i). In 2013, LST values in the study area ranged between 30.97 °C and 41.91 °C, whereas in 2023 they ranged between 26.71 °C and 36.39 °C.

The mean LST decreased from 36.09 °C in 2013 to 31.63 °C in 2023. UHIER calculations were carried out for June, July and August of 2013 and 2023. By averaging the monthly UHIER maps for each year, the annual average UHIER maps were produced. The resulting maps are presented in Fig. 4.(ii). In 2013, UHIER values across the region ranged from −0.17 to 0.15, whereas in 2023, they ranged from −0.17 to 0.11.

As shown in Table 7, there is a marked decrease in the area extent of moderately cooler areas, which dropped from 13% in 2013 to just 5% in 2023. In contrast, slightly warmer areas increased from 23 to 27% and slightly cooler areas increased from 63 to 67% over the same period, which implies a shift from moderately cooler towards either slightly cooler or slightly warmer UHIER groups. This shift indicates a general warming trend in the study area, with formerly cooler zones transitioning toward higher UHIER categories.

The UHIER difference maps, which illustrate the changes in UHIER distribution in the study area over a decade, are shown in Fig. 5. As depicted in the figure, there was an increase in UHIER values in the South-East and North–North-East regions from 2013 to 2023, while a decrease was observed in the South and South-West regions. Figure 5.b presents the reclassified UHIER difference map, where changes are shown by category. The most significant decrease in UHIER values is observed in the West and South-East regions, while the most significant increase is predominantly scattered across the Northern part of the area.

Overall, 64% of the area shows no change in the UHIER (Table 8). Meanwhile, 24% of the area experienced a slight to moderate increase, while 12% experienced a slight to moderate decrease.

Table 9 illustrates the directional changes in the UHIER categories over time. Notably, 77% of the areas classified as moderately cooler in 2013 are projected to shift to slightly cooler areas by 2023, while 67% of the areas classified as moderately warmer in 2013 are expected to transition to slightly warmer areas by 2023.

Table 6 Maximum, Minimum, and Mean Rural LST Values, and Maximum and Minimum UHIER Values for June, July, and August in 2013 and 2023

Year	Month	LST Max (°C)	LST Min (°C)	Mean Rural LST (°C)	UHIER Max	UHIER Min
2013	June	42.45	30.97	36.98	0.15	−0.16
2013	July	44.59	30.81	37.56	0.19	−0.18
2013	August	42.78	29.68	37.53	0.14	−0.21
2023	June	25.66	16.78	19.31	0.30	−0.13
2023	July	41.62	30.18	37.61	0.10	−0.20
2023	August	46.07	32.32	41.83	0.10	−0.20

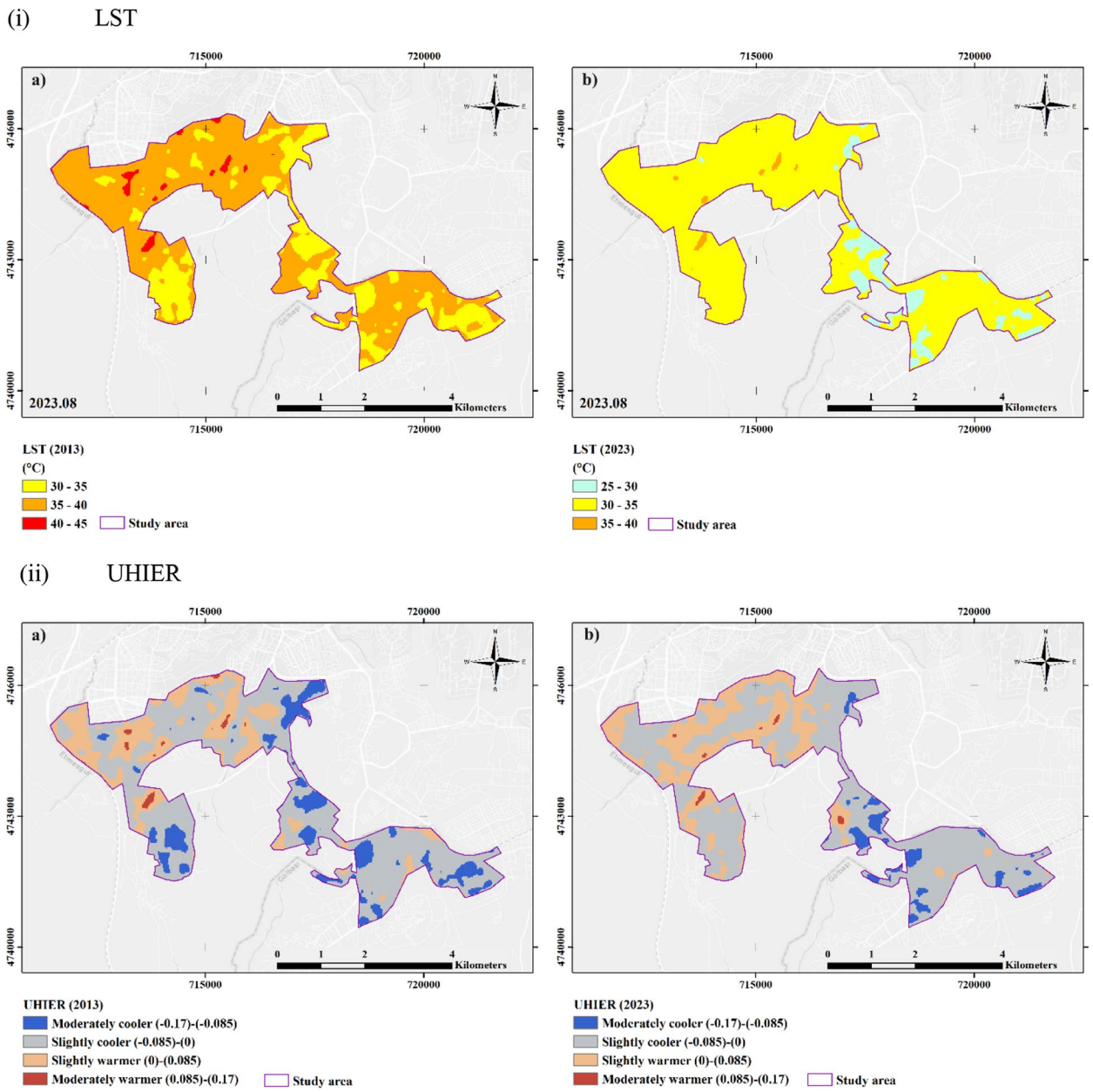


Fig. 4 Spatial distribution of (i) LST and (ii) UHIER across the study area in a) 2013, and b) 2023

Table 7 Area distribution of reclassified maps by UHIER level

UHIER Value	2013		2023	
	Area (ha)	Percent (%)	Area (ha)	Percent (%)
Moderately cooler (−0.17)—(−0.085)	227	13	93	5
Slightly cooler (−0.085)—(0)	1,066	63	1,125	67
Slightly warmer (0)—(0.085)	382	23	463	27
Moderately warmer (0.085)—(0.17)	15	1	9	1
Total	1,690	100	1,690	100

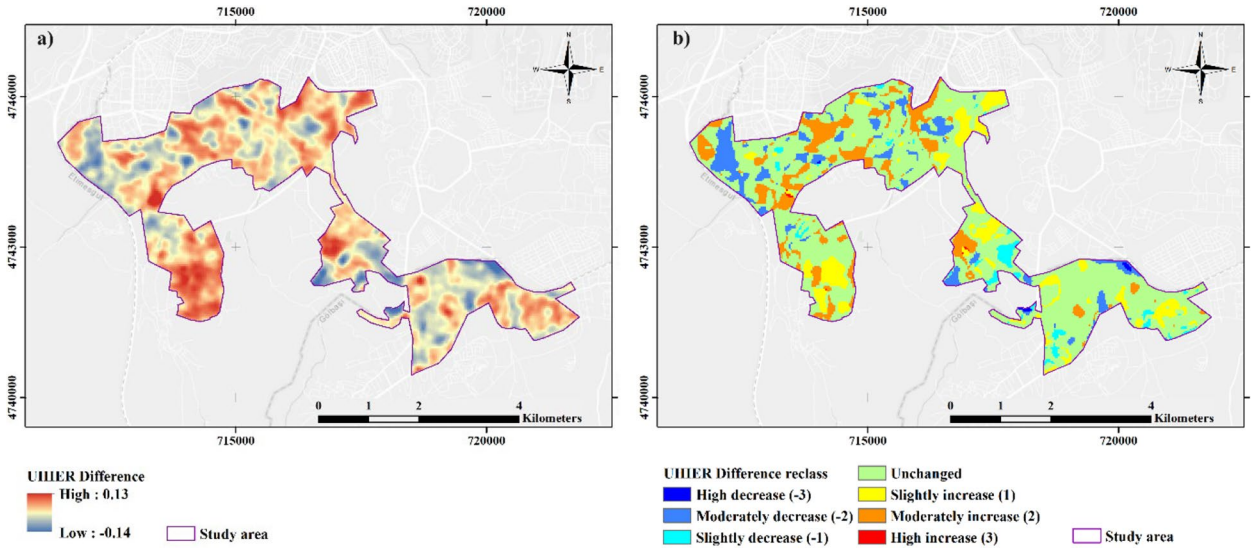


Fig. 5 UHIER difference maps for the study area a) continuous UHIER difference values, and b) reclassified UHIER difference categories indicating cooling and warming intensity

Table 8 Area distribution of UHIER differences

UHIER Difference	Area (ha)	Percent (%)
High decrease (−3)	4	0
Moderately decrease (−2)	148	9
Slightly decrease (−1)	47	3
Unchanged (0)	1,087	64
Slightly increase (1)	177	11
Moderately increase (2)	226	13
High increase (3)	1	0
Total	1,690	100

4.2 LCZ Results

UHIER difference maps, shown in Fig. 6, provide a reference for the degree of change in surface temperatures over a decade. LCZ maps are generated for 2013 and 2023 in order to reveal changes between the two periods, and the study area is extracted from both maps. It is observed that 11 out of 17 LCZ classes are present in the study area in both years. The maps show the spatial distribution of each LCZ categories in both years (Fig. 6). It is observed that the land cover types, particularly low plants, have decreased in size over time, particularly on the eastern part of the study area. Compact land-uses, on the other hand, have tended to increase on the northern part and at the center. Sparesly-built areas have turned to be more prevalent recently.

Table 9 Changes in Area Distribution of UHIER Categories between 2013 and 2023

2013	2023	Area (ha)	Percent (%)	Change
Moderately cooler (−2)	Moderately cooler (−2)	52	23	No change
Moderately cooler (−2)	Slightly cooler (−1)	174	77	Increase
Moderately cooler (−2)	Slightly warmer (1)	1	0	Increase
Slightly cooler (−1)	Moderately cooler (−2)	37	4	Decrease
Slightly cooler (−1)	Slightly cooler (−1)	803	75	No change
Slightly cooler (−1)	Slightly warmer (1)	225	21	Increase
Slightly warmer (1)	Moderately cooler (−2)	4	1	Decrease
Slightly warmer (1)	Slightly cooler (−1)	148	39	Decrease
Slightly warmer (1)	Slightly warmer (1)	227	59	No change
Slightly warmer (1)	Moderately warmer (2)	4	1	Increase
Moderately warmer (2)	Slightly cooler (−1)	0,3	2	Decrease
Moderately warmer (2)	Slightly warmer (1)	10	67	Decrease
Moderately warmer (2)	Moderately warmer (2)	5	31	No change

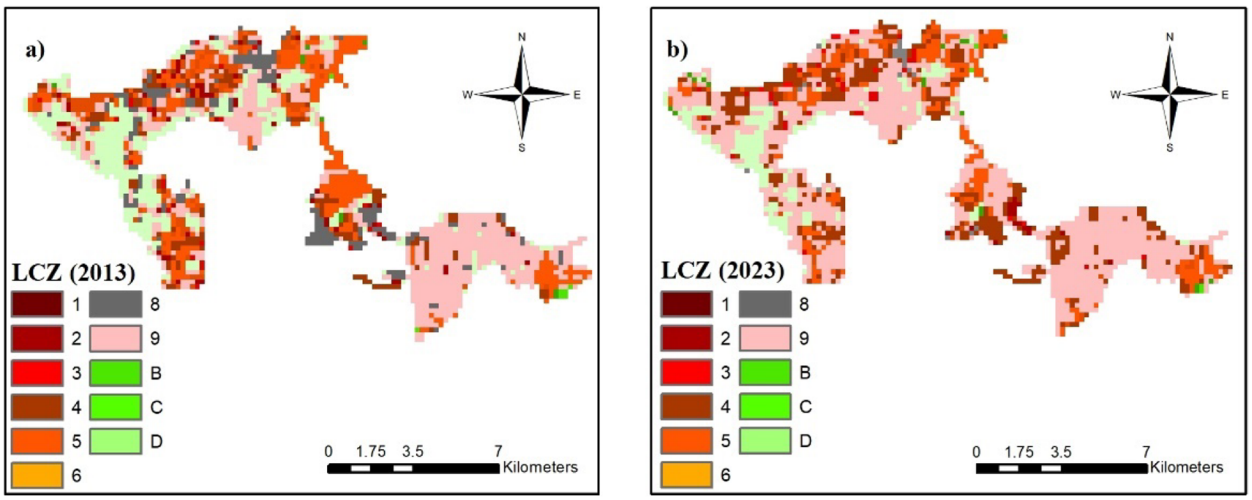


Fig. 6 Spatial distribution of the LCZ categories across the study area in a) 2013 and b) 2023

Table 10 Distribution of LCZ clases in hectares, and their change between 2013 and 2023

LCZ class	2013 (ha)	2023 (ha)	Change (ha)	Change rate
1	3	15	12	3.75
2	47	26	−21	−0.44
3	19	9	−10	−0.52
4	124	307	182	1.47
5	117	43	−74	−0.63
6	305	219	−86	−0.28
8	163	15	−148	−0.91
9	583	888	304	0.52
B	6	13	7	1.13
C	5	2	−2	−0.50
D	324	159	−165	−0.51
Total	1,697	1,697		

The change of the size of each LCZ class is presented in Table 10. It can be concluded that the highest increase has been observed in sparsely built areas (class 9) with an increase of 304 hectares, whereas the highest decrease has been observed in low plants (class D) with a decrease of 165 hectares. When considering change rates, compact high-rise areas (class 1) increased 3.75 times over a decade, whereas only about 9% of large low-rise areas (class 8) remained between the two periods. In general, high-rise developments and sparsely built areas have increased, whereas all other built types have tended to decrease. Besides, all rural land uses, except for scattered trees, have decreased in size.

4.3 Analysis of LCZ changes with regard to UHIER difference groups

To assess the relationship between LCZ transitions and variations in UHIER, a statistical analysis is conducted. To prepare the data for analysis, spatial preprocessing is performed in ArcMap. First, LCZ layers are resampled to match the resolution of the UHIER raster. Point data layers are then created from the UHIER change, LCZ 2013, and LCZ 2023 rasters. After extracting pixel-level UHIER change values, the corresponding LCZ classes are assigned. This process results in a dataset of 18,700 observations covering the entire study area. A new column is created to indicate LCZ transitions from 2013 to 2023 (e.g., class 1 → class 2, class 9 → class 4, class C → class 3, etc.). Since the data do not meet normality assumptions, a Kruskal–Wallis test is applied to determine whether UHIER values differ significantly across LCZ transition categories.

The analysis reveals a statistically significant effect of transition type on UHIER with $H(9) = 50.91$, $p < .001$), indicating that land-use changes are associated with substantial variations in UHIER. Descriptive analysis shows that the highest mean UHIER values occur in transitions such as class C → class 5 ($M = 1.05$), reflecting conversions from bush and scrub to open mid-rise built-up areas increases mean UHIER values. Conversely, transitions such as class C → class 9 ($M = -2.00$), representing changes from bush and scrub to sparsely built areas, exhibit cooling effects. These findings suggest that certain development-driven LCZ transitions substantially amplify UHI intensity, while others may help mitigate it.

Spatial distribution of the LCZ classes in both years are analyzed with regard to the UHIER difference map.

The results of the change in each LCZ class corresponding to each UHIER difference group are shown in Fig. 7.

It can be observed that moderate UHIER increase areas experienced notable changes in terms of the increase in open high-rise and sparsely built areas and the decrease in low plants, all of which are expected to increase the UHI effect. Although compact high-rise areas have increased slightly in size, they can contribute to higher UHI values in the most recent year. Areas with a slight UHIER increase experience similar changes to those with a moderate UHIER increase, but to a lesser degree. The highest UHIER increase and the highest UHIER decrease groups have not experienced significant LCZ changes. It is also important to remind that the highest increase and highest decrease areas are considerably small in size, with about 1 ha and 4 ha, respectively. A large portion of the area remained in the same class in terms of the UHIER groups. In these areas, it can be concluded that

UHIER Difference Group	*Slight increase (+1)*				*Moderate increase (+2)*				*High increase (+3)*			
LCZ Group	2013 (ha)	2023 (ha)	Change (ha)	Change (ha std)	2013 (ha)	2023 (ha)	Change (ha)	Change (ha std)	2013 (ha)	2023 (ha)	Change (ha)	Change (ha std)
1	0.00	1.54	**1.54**	**0.05**	0.00	5.41	**5.41**	**0.17**	0.00	0.00	**0.00**	**0.00**
2	3.09	2.32	**-0.77**	**-0.02**	8.50	10.04	**1.54**	**0.05**	0.00	0.00	**0.00**	**0.00**
3	0.00	0.77	**0.77**	**0.02**	4.63	2.32	**-2.32**	**-0.07**	0.00	0.00	**0.00**	**0.00**
4	21.63	47.88	**26.26**	**0.81**	23.94	51.75	**27.80**	**0.86**	0.00	0.00	**0.00**	**0.00**
5	14.67	4.04	**-10.63**	**-0.33**	24.71	5.72	**-18.99**	**-0.58**	0.00	0.00	**0.00**	**0.00**
6	85.73	65.93	**-19.80**	**-0.61**	34.76	23.03	**-11.72**	**-0.36**	0.77	0.00	**-0.77**	**-0.02**
8	4.63	0.00	**-4.63**	**-0.14**	37.84	8.50	**-29.35**	**-0.90**	0.00	0.00	**0.00**	**0.00**
9	34.76	48.32	**13.57**	**0.42**	48.66	101.18	**52.52**	**1.62**	0.00	0.77	**0.77**	**0.02**
B	*0.00*	*0.00*	**0.00**	***0.00***	*0.00*	*0.00*	**0.00**	***0.00***	*0.00*	*0.00*	**0.00**	***0.00***
C	*0.77*	*0.00*	**-0.77**	***-0.02***	*0.00*	*0.00*	**0.00**	***0.00***	*0.00*	*0.00*	**0.00**	***0.00***
D	*6.95*	*1.54*	**-5.41**	***-0.17***	*40.93*	*16.31*	**-24.63**	***-0.76***	*0.00*	*0.00*	**0.00**	***0.00***
Total	**172.2**	**172.2**	**0.1**	**0.0**	**224.0**	**224.0**	**0.3**	**0.0**	**0.8**	**0.8**	**0.0**	**0.0**
UHIER Difference Group	*Slight decrease (-1)*				*Moderate decrease (-2)*				*High decrease (-3)*			
LCZ Group	2013 (ha)	2023 (ha)	Change (ha)	Change (ha std)	2013 (ha)	2023 (ha)	Change (ha)	Change (ha std)	2013 (ha)	2023 (ha)	Change (ha)	Change (ha std)
1	1.54	2.32	**0.77**	**0.02**	0.00	0.00	**0.00**	**0.00**	0.00	0.00	**0.00**	**0.00**
2	3.86	2.01	**-1.85**	**-0.06**	6.95	3.86	**-3.09**	**-0.09**	0.00	0.00	**0.00**	**0.00**
3	1.54	0.00	**-1.54**	**-0.05**	2.32	0.77	**-1.54**	**-0.05**	0.00	0.00	**0.00**	**0.00**
4	2.32	10.81	**8.50**	**0.26**	11.59	23.94	**12.36**	**0.38**	1.54	3.09	**1.54**	**0.05**
5	0.00	0.00	**0.00**	**0.00**	6.95	3.86	**-3.09**	**-0.09**	0.77	0.00	**-0.77**	**-0.02**
6	3.09	2.54	**-0.54**	**-0.02**	6.18	4.63	**-1.54**	**-0.05**	0.00	0.00	**0.00**	**0.00**
8	11.59	0.00	**-11.59**	**-0.36**	17.76	3.09	**-14.67**	**-0.45**	2.32	0.00	**-2.32**	**-0.07**
9	13.13	20.85	**7.72**	**0.24**	40.93	77.23	**36.30**	**1.12**	0.00	1.54	**1.54**	**0.05**
B	*0.00*	*0.77*	**0.77**	***0.02***	*0.77*	*0.77*	**0.00**	***0.00***	*0.00*	*0.00*	**0.00**	***0.00***
C	*1.54*	*0.00*	**-1.54**	***-0.05***	*0.00*	*0.00*	**0.00**	***0.00***	*0.00*	*0.00*	**0.00**	***0.00***
D	*7.72*	*6.86*	**-0.86**	***-0.03***	*50.97*	*25.94*	**-25.03**	***-0.77***	*0.00*	*0.00*	**0.00**	***0.00***
Total	**46.3**	**46.3**	**-0.2**	**0.0**	**144.4**	**144.1**	**-0.3**	**0.0**	**4.6**	**4.6**	**0.0**	**0.0**

UHIER Difference Group	*No change*			
LCZ Group	2013 (ha)	2023 (ha)	Change (ha)	Change (ha std)
1	1.54	5.41	**3.86**	**0.12**
2	24.71	8.04	**-16.67**	**-0.51**
3	10.81	5.41	**-5.41**	**-0.17**
4	63.33	169.14	**105.81**	**3.26**
5	70.28	29.63	**-40.66**	**-1.25**
6	174.55	123.21	**-51.34**	**-1.58**
8	88.82	3.86	**-84.96**	**-2.61**
9	445.64	637.60	**191.96**	**5.91**
B	*5.41*	*11.59*	**6.18**	***0.19***
C	*2.32*	*2.32*	**0.00**	***0.00***
D	*217.03*	*108.13*	**-108.90**	***-3.35***
Total	**1104.4**	**1104.4**	**-0.1**	**0.0**

Fig. 7 The areas of LCZs and their change in 2013–2023 period in relation to corresponding UHIER difference group

the increases in open high-rise and sparsely built may cancel out the decrease in other built types as well as the increase in scattered trees. The decrease in large low-rise also considered to play an important role in preventing these areas from experiencing increased UHI values. Areas with UHIER decrease, on the other hand, do not have dramatic LCZ changes. The decrease in large low-rise seems to have a positive impact on keeping UHI at lower levels in spite of the increase in open high-rise and sparsely built areas. Moreover, compact high-rise is almost not evident in UHIER decrease groups.

These patterns reveal that specific LCZ transitions have meaningful implications for the UHIER variations. The area is predominantly characterized by three LCZ types: open high-rise, open low-rise and sparsely built land uses. In particular, the increase in open high-rise and sparsely built areas, both of which typically involve high surface exposure, can intensify local heat retention, especially when not mitigated by green infrastructure. In contrast, open low-rise appears to mitigate UHI impacts, likely due to its planned low-rise, low-density development pattern complemented by landscaping features.The observed reduction in low plants further suggests a shift toward more susceptibility to rising UHI effects. Although compact high-rise areas expanded only slightly, their high density and surface properties exacerbate UHI conditions. Furthermore, the relative stability of UHIER in most areas, despite small-scale LCZ changes, implies that the balance between increasing and decreasing built-up forms plays a critical role in regulating local temperatures. The absence of dramatic LCZ shifts in UHIER decrease areas suggests that thermal improvement can occur even without large-scale land cover change, possibly through subtle shifts in building typology or vegetation presence. These findings highlight the need to consider both the type and spatial configuration of LCZs in urban planning efforts aimed at mitigating UHI related concerns, particularly in areas where urban development and construction are ongoing.

5 Discussion

Urban development patterns of 2013 and 2023 are compared with regard to the changes in UHI and LCZC for the southwestern fringe of Ankara. The results show that the areas experiencing high UHIER increase and high UHIER decrease are negligible since they cover less than 0.2% of the total area. Moderate decrease and moderate increase areas cover 9% and 13% of the entire area, respectively, while slight decrease and slight increase cover 3% and 11% or the entire area, respectively. It is evident that the groups associated with UHIER increase surpass those associated with UHIER decrease. The overall UHIER increase encompasses nearly one-quarter of the study area, which is approximately twice the extent of the overall UHIER decrease, covering 12% of the area. The largest part of the study area remains unchanged in terms of the UHIER values, covering 64% of the area. When the UHIER changes are investigated in detail, the largest trasformation, covering 225 hectares, has been observed from slightly cooler to slightly warmer, followed by 172 hectares transformed from moderately cooler to slightly cooler. These two largest transformation areas indicate UHIER increase. The third largest transformation, on the other hand, covers 148 hectares, where slightly warmer areas have become slightly cooler.

LCZ transformations have also been analyzed to understand the potential impact of land use changes. In this study, LCZ mapping was conducted using the WUDAPT protocol, grounded in the classification framework proposed by Stewart and Oke (2012) and implemented in accordance with the methodological guidelines outlined by Demuzere et al. (2021). The LCZ classification used in this study is based on the WUDAPT framework, which is a recognized tool in urban climate literature (Ching et al., 2018; Mushore et al., 2022; Rahmani & Sharifi, 2023). LCZ maps for Ankara were derived from the WUDAPT-generated outputs for 2013 and 2023. The results confirm an overall increase in built types. The most significant change rate is observed in compact high-rise areas, with a 3.75 times increase. The following highest rate is observed in open high-rise areas, with a 1.47 times increase. When the size of each LCZ change is considered, the largest change is observed in sparsely built areas, with an incresae of 304 hectares, followed by open high-rise areas, with an increase of 182 hectares. Low plants, on the other hand, decreased by around 165 hectares. Such increase in built types and decrease in land cover is considered to play a role in increasing UHIER values in the area. The spatial correspondances of the UHIER changes and the LCZ changes are also informative.

Higher UHIER increase and higher UHIER decrease areas do not reflect significant LCZC changes. They are also quite small areas in size, therefore, can be neglected. Moderate UHIER increase areas experienced considerable increases in open high-rise and sparsely built classes, accompanied with a decrease in low plants. Such changes appear to offset the potential UHIER decrease from reduction of open mid-rise, open low-rise and large low-rise areas. Additionally, the most evident increase in compact high-rise is observed in this UHIER group. The results are in line with the findings in the literature, indicating that LCZs dominated by dense high-rise structures exhibite higher temperatures, whereas areas with vegetation are more effective in reducing heat (Chen et al., 2023; Herath et al., 2018; Nastran et al.,

2019; Ogce et al., 2025; Rahmani & Sharifi, 2023). Slight UHIER increase areas also reflect a similar pattern, with lower intensities. The results support the findings in the literature indicating LCZ of built-up leads to higher UHI values than the natural ones (Shi, et al., 2022). The areas without UHIER change experience significant changes almost in all groups, such as increasing open high-rise and sparsely built areas and decreasing large low rise and low plant areas. Moreover, the only increase in scattered trees is observed in this group, although not quite significant. It can be concluded that although compact high-rise, open high-rise, and sparsely built areas have increased, the decrease in other built-types, particularly large low-rise, and the increase in tree density seem to balance the UHIER changes. As indicated in Ananyeva and Emmanuel (2023), vegetation plays an important role in reducing surface temperatures, with trees offering greater potential for cooling than shrubs and grass. Trees and greenery at the ground level are found to be decreasing overheating of urban areas (Khan et al., 2023). A tree canopy exhibits stronger cooling potential due to its shading effect (Hou & Estoque, 2020), while they increase local breezes in urban areas (Yilmaz & Ozturk, 2024). Slightly or moderately decreased UHIER groups do not reflect a significant LCZ change except for large low-rise group. Decreasing large low-rise is related to various building sites of the previous period, which turned into built-up areas in the latter period. However, if the intention is to keep UHIER at lower levels, the expansion of compact high-rise and open high rise areas should be limited. Similarly, the expansion of the sparsely built areas appears to use land inefficiently, which has an increasing impact on UHI values and should be limited. Moreover, areas should be reserved for land covers such as scattered trees.

When the LCZ-UHI relationship is considered, most previous studies have focused on established built-up areas and there are fewer studies investigating the effects of macroform changes in urban development areas. The results of this study align with findings from Dimitrov's (2021) research on urban expansion in Sofia, which also highlighted the role of open high-rise and sparsely built areas in contributing to elevated UHI values. In both studies, low plants were found to mitigate heat effects. Our results also support the outcomes of ground-based thermal surveys by confirming similar patterns using satellite-derived imagery, thereby reinforcing their validity through an alternative methodology. Unlike the findings of Mushore et al. (2022), Lee et al. (2024), and Zhang et al., (2021a, 2021b), where economic or industrial activities represented by LCZ types such as large low-rise and lightweight low-rise played a significant role in urban development areas, our study area is primarily characterized by residential land use types. This distinction allows us to better observe how variations in different LCZ types related to residential macroform influence UHIER, while the dominance of residential LCZ types in our study area makes it possible to isolate and interpret the thermal effects of residential land-use patterns more clearly.

The results highlight that the observed increase in UHIER is primarily associated with the expansion of open high-rise and sparsely built LCZs, coupled with the reduction of open green areas, rather than being driven solely by localized pixel-level transitions. This overall shift in the composition of the urban fabric reflects the ongoing urbanization of the southwestern fringe, where the increase in built-up surfaces and the loss of vegetated cover have collectively contributed to heat intensification. These findings confirm that urban development dynamics and LULC changes play a critical role in shaping spatial UHI patterns. This pixel-level approach strengthens the interpretation of spatial heterogeneity in UHIER and provides an evidence-based foundation for targeted planning interventions in heat-sensitive areas.

Considering the findings within the context of current planning and development strategies, it becomes evident that existing policies provide only partial guidance for UHI mitigation in Ankara. At the national level, the Climate Change Mitigation Strategy and Action Plan (2024–2030) by the Ministry of Environment, Urbanization and Climate Change (The Ministry of Environment, Urbanization and Climate Change, 2023) emphasizes the expansion of green spaces in urban areas as part of climate adaptation goals, yet it does not explicitly address UHI dynamics. At the local level, the Ankara Local Climate Change Action Plan (Ankara Greater Municipality, (2022) highlights vegetation and green infrastructure as the primary tools for reducing UHI intensity, recommending both the expansion of open green space systems and micro-scale interventions such as green roofs. However, the Territorial Development Plan of Ankara (Ankara Greater Municipality, (2007), which designates the southeastern development corridor, including the study area, as predominantly residential, does not refer to UHI or green infrastructure in the study area. The plan anticipates significant population growth and building density in the corridor, while fragmented green space allocations in newly developing residential zones create both spatial discontinuity and financial challenges for the municipality in implementing and maintaining green infrastructure.

In the context of Ankara's insufficient policy framework, this study provides evidence-based insights that can inform local development strategies for mitigating UHI impacts. The results provide

evidence-based insights for local planning. Findings suggest that rapidly urbanizing areas with increasing open high-rise, compact high-rise, and scattered built forms are major contributors to UHIER intensification, whereas promoting open low-rise typologies integrated with larger, contiguous green spaces can effectively mitigate UHI effects. Therefore, a more integrated urban development strategy that coordinates macroform decisions with continuous, multi-scaled green infrastructure is essential for sustainable thermal management in Ankara's developing urban fringe.

6 Limitations

LCZ mapping is conducted for an entire city for a specific time. Therefore, the accuracy of the LCZ map reflects the level of confidence in the classification for the entire area as well, but local accuracies may vary. Class probabilities provided by the WUDAPT protocol are considered an accuracy measeure for the sub-sections of the entire region of interest. The global accuracy may also vary accross different years. In this study, the accuracy for 2013 is lower than that for 2023. When the accuracies of the LCZ classes are investigated, the lowest accuracy for 2013 appears to be observed in compact low-rise. This issue appears to stem from the prevalence of squatter settlements, which are challenging to define due to their small sizes and clustering patterns. These irregular settlements consisting of several tiny housing units clustered together in topographically disadvantaged areas such as steep slopes, have varying horizontal and vertical profiles. This variability makes it difficult to determine their densities. Moreover, in some instances some of these settlements are incorrectly classified as bush and scrub due to their small sizes and the presence of trees covering housing units. However, it is important to emphasize that such irregular settlements were absent in the study area in both years, implying that the classification accuracy for this area is likely higher than for the rest of the city. Another limitation of the study is the incompatibility of raster data resolutions of different data. Even when re-projected to the same resolution, the total area of the initial data remains unchanged. UHIER data derived from Landsat 8 imagery has a resolution of 30 m x 30 m in the WGS 1984 UTM Zone 36N projection. LCZ data, provided without a projection, has a default resolution of 87.88 m × 87.88 m resolution when projected to WGS 1984 UTM Zone 36N. Consequently, their study area totals do not match: the former covers 1,690 hectares, while the latter covers 1,697 hectares. However, a deviation of 0.4% is considered negligible.

7 Conclusions

Addressing the gap in existing upper-scale guiding plans, this study delivers empirical evidence on the UHI issue and provides a basis for formulating potential policy recommendations. This study provided an in-depth assessment of the relationship between land use transformation and UHI dynamics, specifically quantified through UHIER, in the southwestern urban development area of Ankara between 2013 and 2023. Utilizing RS and GIS techniques in conjunction with the WUDAPT protocol, the analysis demonstrated how shifts in LCZ types—driven by urban expansion, densification, and changes in surface materials—directly influence UHIER variability across space and time. The increase in impervious surfaces, reduction in vegetated zones, and increasing built-up densities are shown to be the primary drivers of increased LST and intensified UHI effects.

The spatial analysis revealed that moderately and slightly increasing UHIER zones occupy a substantially larger area than those experiencing decreases. These increase parts are closely associated with growing open high-rise and sparsely built LCZ types, accompanied by a decrease in low plant cover, predominantly grasslands. Such a pattern suggests that increasing densities alone are not the sole determinant of thermal intensification—rather, the type and spatial structure of the urban form, in combination with surface properties, play a crucial role. Conversely, moderate and slight UHIER decrease areas were strongly correlated with reductions in large low-rise developments. This finding implies that horizontal urban forms with lower densities and greater integration with green infrastructure may contribute to the mitigation of UHI effects. The analysis also highlighted that a significant portion of the study area did not exhibit major UHIER change over the decade. However, LCZ transitions were still evident in these comparably stable zones, including marked reductions in compact mid-rise, open mid-rise, and large low-rise areas. These findings underscore that even in locations where UHIER values remain static, ongoing land use restructuring can have latent implications for future thermal conditions, especially if green elements are not adequately preserved or replaced.

The role of vegetation, particularly tree cover, emerged as a vital moderating factor. As emphasized in the literature, tree canopies provide greater cooling potential than shrubs or grasses due to their height, evapotranspiration capacity, and shading effect. In the study area, a modest increase in scattered trees was observed, which likely mitigated some of the heat stress

induced by the loss of low plants. Nonetheless, this increase appears insufficient to fully counterbalance the widespread decline in vegetated areas, particularly given the scale of urban development. From a planning perspective, the results highlight the importance of prioritizing climate-sensitive urban development strategies. These include integrating tree-based green infrastructure, limiting the expansion of high-rise and impervious surfaces, and promoting mid- and low-rise forms that enable the preservation of pervious surfaces and vegetated zones. Efficient land use planning that balances densification with ecological considerations is essential to maintain thermal comfort, reduce energy demand, and improve urban resilience in the face of climate change. Future research could build on these findings by integrating temporal LST series, high-resolution LCZ mapping, and socio-economic variables to capture not only the physical but also the behavioral and policy-driven dimensions of UHI change. Such a multi-dimensional approach would further strengthen urban climate adaptation strategies, particularly for rapidly developing urban fringes like the one analyzed in this study.

Authors' contributions

All authors contributed to the study's conception and design. Material preparation, data collection, and UHIER analysis were carried out by Mehtap Ozenen-Kavlak, while the method was developed by Muzeyyen Anil Senyel Kurkcuoglu and Mehtap Ozenen-Kavlak. LCZ analysis was conducted by Muzeyyen Anil Senyel Kurkcuoglu. The first draft of the manuscript was written by Muzeyyen Anil Senyel Kurkcuoglu, Mehtap Ozenen-Kavlak, Halil Duymus and Saye Nihan Cabuk, and the editing was provided by Muzeyyen Anil Senyel Kurkcuoglu. All authors provided feedback on previous versions of the manuscript. All authors have read and approved the final manuscript.

Funding

The authors declare that no funds, grants, or other support were received during the preparation of this manuscript.

Data availability

Data will be made available on reasonable request.

Declarations

Competing Interests

The authors have no relevant financial or non-financial interests to disclose.

Received: 20 June 2025 Revised: 1 August 2025 Accepted: 3 August 2025
Published online: 15 August 2025

References

Acosta-Fernandez, G. A., Martinez-Torres, K. E., & Gonzalez-Trevizo, M. E. (2025). Advances in urban mapping of local climate zones for heat mitigation: a systematic review. Land Use Policy. https://doi.org/10.1016/j.landusepol.2025.107540

Aik, D. H. J., Ismail, M. H., & Muharam, F. M. (2020). Land use/land cover changes and the relationship with land surface temperature using Landsat and MODIS imageries in Cameron Highlands, Malaysia. Land. https://doi.org/10.3390/land9100372

Ananyeva, O., & Emmanuel, R. (2023). Street trees and Urban Heat Island in Glasgow: Mitigation through the 'Avenues Programme.' *Urban Forestry & Urban Greening*. https://doi.org/10.1016/j.ufug.2023.128041

Ankara Greater Municipality (2007) Ankara 1:25000 Master Plan. Retrieved 24 July 2025 from https://www.ankara.bel.tr/ankara-buyuksehir-belediyesi-nazim-plan

Ankara Greater Municipality (2022) Ankara Local Climate Change Action Plan. Retrieved 24 July 2025 from https://www.ankara.bel.tr/files/2022/06/22/0b663954d523bfee1d1e1d5fa66a082f.pdf

Atasoy, M. (2020). Assessing the impacts of land-use/land-cover change on the development of urban heat island effects. *Environment, Development and Sustainability*. https://doi.org/10.1007/s10668-019-00535-w

Badaro-Saliba, N., Adjizian-Gerard, J., Zaarour, R., & Najjar, G. (2021). Lcz scheme for assessing urban heat island intensity in a complex urban area (Beirut, Lebanon). *Urban Climate*. https://doi.org/10.1016/j.uclim.2021.100846

Bechtel, B., Demuzere, M., Mills, G., et al. (2019). SUHI analysis using local climate zones—A comparison of 50 cities. *Urban Climate*. https://doi.org/10.1016/j.uclim.2019.01.005

Cetin M, Isik Pekkan Ö, Ozenen Kavlak M, et al (2022) GIS-based forest fire risk determination for Milas district, Turkey. Natural Hazards. https://doi.org/10.1007/s11069-022-05601-7

Cetin M, Ozenen Kavlak M, Senyel Kurkcuoglu MA, et al (2024) Determination of land surface temperature and urban heat island effects with remote sensing capabilities: the case of Kayseri, Türkiye. Natural Hazards. https://doi.org/10.1007/s11069-024-06431-5

Chen, G., Chen, Y., Tan, X., Zhao, L., Cai, Y., & Li, L. (2023). Assessing the urban heat island effect of different local climate zones in Guangzhou, China. *Building and Environment*. https://doi.org/10.1016/j.buildenv.2023.110770

Chen, X. L., Zhao, H. M., Li, P. X., & Yin, Z. Y. (2006). Remote sensing image-based analysis of the relationship between urban heat island and land use/cover changes. *Remote Sensing of Environment*. https://doi.org/10.1016/j.rse.2005.11.016

Ching, J., Mills, G., Bechtel, B., et al. (2018). WUDAPT: An urban weather, climate, and environmental modeling infrastructure for the anthropocene. *Bulletin of the American Meteorological Society*. https://doi.org/10.1175/BAMS-D-16-0236.1

Dağlıoğlu, E. (2024). Mimarlığın Nesnesi Olarak Kenti Yeniden Arzulamak: Ankara'nın Kentsel Yayılma Pratikleri ve Çeper Mimarisi Üzerine Spekülatif Bir Okuma. *Mimarlık Dergisi, 439*, 30–36.

Demuzere, M., Kittner, J., & Bechtel, B. (2021). Lcz generator: A web application to create local climate zone maps. *Frontiers in Environmental Science*. https://doi.org/10.3389/fenvs.2021.637455

Dimitrov, S., Popov, A., & Iliev, M. (2021). An application of the LCZ approach in surface urban heat island mapping in Sofia, Bulgaria. *Atmosphere, 12*(11), Article 1370. https://doi.org/10.3390/atmos12111370

Ding, H., & Shi, W. (2013). Land-use/land-cover change and its influence on surface temperature: A case study in Beijing City. *International Journal of Remote Sensing*. https://doi.org/10.1080/01431161.2013.792966

Du, H., Zhou, F., Li, C., et al. (2020). Analysis of the impact of land use on spatiotemporal patterns of surface urban heat island in rapid urbanization, a case study of Shanghai, China. *Sustainability*. https://doi.org/10.3390/su12031171

Elliot, T., Babí Almenar, J., & Rugani, B. (2020). Modelling the relationships between urban land cover change and local climate regulation to estimate urban heat island effect. *Urban Forestry & Urban Greening*. https://doi.org/10.1016/j.ufug.2020.126650

Estoque, R. C., Murayama, Y., & Myint, S. W. (2017). Effects of landscape composition and pattern on land surface temperature: An urban heat island study in the megacities of Southeast Asia. *Science of the Total Environment*. https://doi.org/10.1016/j.scitotenv.2016.10.195

Falah, N., Solis-Guzman, J., & Falah, N. (2024). Thermal footprint of the urbanization process: Analyzing the heat effects of the Urbanization Index (UI) on the Local Climate Zone (LCZ) and Land Surface Temperature (LST) over two decades in Seville. *Land, 13*(11), 1877. https://doi.org/10.3390/land13111877

Feng, H., Zhao, X., Chen, F., & Wu, L. (2014). Using land use change trajectories to quantify the effects of urbanization on urban heat island. *Advances in Space Research*. https://doi.org/10.1016/j.asr.2013.11.028

Garzón, J., Molina, I., Velasco, J., & Calabia, A. (2021). A remote sensing approach for surface urban heat island modeling in a tropical Colombian city using regression analysis and machine learning algorithms. *Remote Sensing, 13*(21), 4256. https://doi.org/10.3390/rs13214256

Gee OK, Sarker MLR (2013) Monitoring the effects of land use/landcover changes on urban heat island. In: Earth Resources and Environmental Remote Sensing/GIS Applications IV

Guindon, S. M., & Nirupama, N. (2015). Reducting risk from urban heat island effects in cities. *Natural Hazards*. https://doi.org/10.1007/s11069-015-1627-8

Güneş P (2021) Assessment of Relationship Between Urban Growth, Urban Sprawl, Urban Fringe and Real Estate Markets: The case of Alacaatlı, Bağlıca and Dodurga Neighborhoods of Ankara, Unpublished Master's Thesis, Ankara University.

Halder, B., Karimi, A., Mohammad, P., et al. (2022). Investigating the relationship between land alteration and the urban heat island of Seville city using multi-temporal Landsat data. *Theoretical and Applied Climatology*. https://doi.org/10.1007/s00704-022-04180-8

Hasanlou M, Mostofi N (2015) Investigating urban heat island estimation and relation between various land cover indices in Tehran city using Landsat 8 imagery. In: Proceedings of the 1st International Electronic Conference on Remote Sensing. Basel, Switzerland

Herath, H. M. P. I. K., Halwatura, R. U., & Jayasinghe, G. Y. (2018). Evaluation of green infrastructure effects on tropical Sri Lankan urban context as an urban heat island adaptation strategy. *Urban Forestry & Urban Greening*. https://doi.org/10.1016/j.ufug.2017.11.013

Hoan, N. T., Liou, Y. A., Nguyen, K. A., et al. (2018). Assessing the effects of land-use types in surface urban heat islands for developing comfortable living in Hanoi City. *Remote Sensing, 10*, Article 1965. https://doi.org/10.3390/rs10121965

Hou, H., & Estoque, R. C. (2020). Detecting cooling effect of landscape from composition and configuration: An urban heat island study on Hangzhou. *Urban Forestry & Urban Greening*. https://doi.org/10.1016/j.ufug.2020.126719

Hu, Y., & Jia, G. (2010). Influence of land use change on urban heat island derived from multi-sensor data. *International Journal of Climatology, 30*, 1382–1395. https://doi.org/10.1002/joc.1984

Huang, Q., Huang, J., Yang, X., et al. (2019). Quantifying the seasonal contribution of coupling urban land use types on urban heat island using land contribution index: A case study in Wuhan, China. *Sustainable Cities and Society*. https://doi.org/10.1016/j.scs.2018.10.016

Ishibashi, K., Ota, S., Yokoyama, M., et al. (2019). Evaluating land use scenario with population decreasing from the viewpoint of urban heat island mitigation: A study in the major cities in Chugoku region. *Journal of Environmental Engineering (Transactions of AIJ)*. https://doi.org/10.3130/aije.84.771

Kamali Maskooni, E., Hashemi, H., Berndtsson, R., et al. (2021). Impact of spatiotemporal land-use and land-cover changes on surface urban heat islands in a semiarid region using Landsat data. *International Journal of Digital Earth*. https://doi.org/10.1080/17538947.2020.1813210

Kardinal Jusuf, S., Wong, N. H., Hagen, E., et al. (2007). The influence of land use on the urban heat island in Singapore. *Habitat International,31*, 232–242. https://doi.org/10.1016/j.habitatint.2007.02.006

Keith, L., Gabbe, C. J., & Schmidt, E. (2023). Urban heat governance: Examining the role of urban planning. *Journal of Environmental Policy and Planning*. https://doi.org/10.1080/1523908X.2023.2244446

Khan, A., Carlosena, L., Khorat, S., Khatun, R., Das, D., Doan, Q., Hamdi, R., Aziz, M., Hashem, A., Santamouris, M., & Niyogi, D. (2023). Urban cooling potential and cost comparison of heat mitigation techniques for their impact on the lower athmosphere. *Computational Urban Science, 3*, 26. https://doi.org/10.1007/s43762-023-00101-1

Kim, J. P., & Guldmann, J. M. (2014). Land-use planning and the urban heat island. *Environment and Planning b, Planning & Design*. https://doi.org/10.1068/b130091p

Kong, G., Peng, J., & Corcoran, J. (2025). Modelling urban heat island effects: A glocal analysis of 216 cities using machine learning techniques. *Computational Urban Science,5*, Article 18. https://doi.org/10.1007/s43762-025-00178-w

Kumar, B. P., Babu, K. R., Anusha, B. N., & Rajasekhar, M. (2022). Geo-environmental monitoring and assessment of land degradation and desertification in the semi-arid regions using Landsat 8 OLI / TIRS, LST, and NDVI approach. *Environmental Challenges, 8*, Article 100578. https://doi.org/10.1016/j.envc.2022.100578

Lau, K. K. L., Chung, S. C., & Ren, C. (2019). Outdoor thermal comfort in different urban settings of sub-tropical high-density cities: An approach of adopting local climate zone (LCZ) classification. *Building and Environment*. https://doi.org/10.1016/j.buildenv.2019.03.005

Leconte, F., Bouyer, J., Claverie, R., & Pétrissans, M. (2015). Using local climate zone scheme for UHI assessment: Evaluation of the method using mobile measurements. *Building and Environment, 83*, 39–49. https://doi.org/10.1016/j.buildenv.2014.05.005

Lee, K., Yoo, C., & Park, S. (2024). Differences in LCZ composition according to urban planning and impacts on urban thermal environment. *Energy and Buildings, 314*, Article 114272. https://doi.org/10.1016/j.enbuild.2024.114272

Li, C. F., & Yin, J. Y. (2013). A study on urban thermal field of Shanghai using multi-source remote sensing data. *Journal of the Indian Society of Remote Sensing*. https://doi.org/10.1007/s12524-013-0268-1

Li, C., Shen, D., Dong, J., et al. (2014). Monitoring of urban heat island in Shanghai, China, from 1981 to 2010 with satellite data. *Arabian Journal of Geosciences*. https://doi.org/10.1007/s12517-013-1053-8

Li, F., Yigitcanlar, T., Nepal, M., Thanh, K. N., & Dur, F. (2024). A novel urban heat vulnerability analysis: Integrating machine learning and remote sensing for enhanced insights. *Remote Sensing, 16*(16), 3032. https://doi.org/10.3390/rs16163032

Liang, C., Zhang, R. C., Zeng, J., & Shen, Z. J. (2021). A land-use decision approach integrating thermal regulation, stormwater management, and economic benefits based on urbanization stage identification. *Science of the Total Environment*. https://doi.org/10.1016/j.scitotenv.2021.146415

Liu, K., Su, H., Li, X., et al. (2016). Quantifying spatial-temporal pattern of urban heat island in Beijing: An improved assessment using land surface temperature (LST) time series observations from LANDSAT, MODIS, and Chinese New Satellite GaoFen-1. *IEEE Journal of Selected Topics in Applied Earth Observations and Remote Sensing*. https://doi.org/10.1109/JSTARS.2015.2513598

Liu, S., Zhang, J., Li, J., Li, Y., Zhang, J., & Wu, X. (2021). Simulating and mitigating extreme urban heat island effects in a factory area based on machine learning. *Building and Environment, 202*, Article 108051. https://doi.org/10.1016/j.buildenv.2021.108051

Liu, Y., An, Z., & Ming, Y. (2024). Simulating influences of land use/land cover composition and configuration on urban heat island using machine learning. *Sustainable Cities and Society, 108*, Article 105482. https://doi.org/10.1016/j.scs.2024.105482

Lyu, F., Wang, S., Han, S. Y., et al. (2022). An integrated cyberGIS and machine learning framework for fine-scale prediction of urban heat island using satellite remote sensing and urban sensor network data. *Urban Info, 1*, 6. https://doi.org/10.1007/s44212-022-00002-4

MacLachlan, A., Biggs, E., Roberts, G., & Boruff, B. (2021). Sustainable city planning: A data-driven approach for mitigating urban heat. *Frontiers in the Built Environment*. https://doi.org/10.3389/fbuil.2020.519599

Mushore, T. D., Mutanga, O., & Odindi, J. (2022). Determining the influence of long term urban growth on surface urban heat islands using local climate zones and intensity analysis techniques. *Remote Sensing, 14*(9), 2060. https://doi.org/10.3390/rs14092060

Nakata-Osaki, C. M., Souza, L. C. L., & Rodrigues, D. S. (2018). This – Tool for heat island simulation: A GIS extension model to calculate urban heat island intensity based on urban geometry. *Computers, Environment and Urban Systems*. https://doi.org/10.1016/j.compenvurbsys.2017.09.007

Nastran, M., Kobal, M., & Eler, K. (2019). Urban heat islands in relation to green land use in European cities. *Urban Forestry & Urban Greening*. https://doi.org/10.1016/j.ufug.2018.01.008

Ogce, S., Ogce, H., Yu, S., & Brown, R. D. (2025). The interaction between urban heat island and urban parks: An in-situ measurement-based review. *Land Use Policy*. https://doi.org/10.1016/j.landusepol.2025.107628

Oke, T. R. (1973). City size and the urban heat island. *Atmospheric Environment (1967)*. https://doi.org/10.1016/0004-6981(73)90140-6

Onishi, A., Cao, X., Ito, T., et al. (2010). Evaluating the potential for urban heat-island mitigation by greening parking lots. *Urban Forestry & Urban Greening*. https://doi.org/10.1016/j.ufug.2010.06.002

Pan, J. (2016). Area delineation and spatial-temporal dynamics of urban heat island in Lanzhou city, China using remote sensing imagery.

Journal of the Indian Society of Remote Sensing. https://doi.org/10.1007/s12524-015-0477-x

Parvar, Z., Mohammadzadeh, M., & Saeidi, S. (2024). LCZ framework and landscape metrics: Exploration of urban and peri-urban thermal environment emphasizing 2/3D characteristics. *Building and Environment*. https://doi.org/10.1016/j.buildenv.2024.111370

Peiro M N, Sanchez C S, Gonzalez F J N (2019) Source area definition for local climate zone studies: A systematic review: Build Environ 148: https://doi.org/10.1016/j.buildenv.2018.10.050

Portela, C. I., Massi, K. G., Rodrigues, T., & Alcântara, E. (2020). Impact of urban and industrial features on land surface temperature: Evidences from satellite thermal indices. *Sustainable Cities and Society*. https://doi.org/10.1016/j.scs.2020.102100

Rahmani, N., & Sharifi, A. (2023). Comparative analysis of the surface urban heat island (SUHI) effect based on the local climate zone (LCZ) classification scheme for two Japanese cities, Hiroshima, and Sapporo. *Climate, 11*(7), 142. https://doi.org/10.3390/cli11070142

Rahmani, N., & Sharifi, A. (2025). Urban heat dynamics in local climate zones (LCZs): A systematic review. *Building and Environment*. https://doi.org/10.1016/j.buildenv.2024.112225

Rizwan, A. M., Dennis, L. Y. C., & Liu, C. (2008). A review on the generation, determination and mitigation of urban heat island. *Journal of Environmental Sciences*. https://doi.org/10.1016/S1001-0742(08)60019-4

Salam, M., Islam, M. K., Jahan, I., & Chowdhury, M. A. (2024). Assessing the impacts of vegetation loss and land surface temperature on surface urban heat island (SUHI) in Gazipur district, Bangladesh. *Computational Urban Science, 4*, Article 24. https://doi.org/10.1007/s43762-024-00136-y

Seletković A, Kičić M, Ančić M, et al (2023) The Urban Heat Island Analysis for the City of Zagreb in the Period 2013–2022 Utilizing Landsat 8 Satellite Imagery. Sustainability (Switzerland) 15:. https://doi.org/10.3390/su15053963

Sharifi, E., & Lehmann, S. (2014). Comparative analysis of surface urban heat island effect in central Sydney. *Journal of Sustainable Development, 7*, Article doi: 10.5539/jsd.v7n3p23.

Sheng, L., Tang, X., You, H., et al. (2017). Comparison of the urban heat island intensity quantified by using air temperature and Landsat land surface temperature in Hangzhou, China. *Ecological Indicators*. https://doi.org/10.1016/j.ecolind.2016.09.009

Shi, H., Xian, G., Auch, R., et al. (2021). Urban heat island and its regional impacts using remotely sensed thermal data—a review of recent developments and methodology. *Land*. https://doi.org/10.3390/land10080867

Shi, Z., Yang, J., Zhang, Y., et al. (2022). Urban ventilation corridors and spatiotemporal divergence patterns of urban heat island intensity: A local climate zone perspective. *Environmental Science and Pollution Research, 29*, 74394–74406. https://doi.org/10.1007/s11356-022-21037-9

Stewart, I. D., & Oke, T. R. (2012). Local climate zones for urban temperature studies. *Bulletin of the American Meteorological Society*. https://doi.org/10.1175/BAMS-D-11-00019.1

Tang, J., Di, L., Xiao, J., et al. (2017). Impacts of land use and socioeconomic patterns on urban heat island. *International Journal of Remote Sensing*. https://doi.org/10.1080/01431161.2017.1295485

The Ministry of Environment, Urbanization and Climate Change (2023) Climate Change Mitigation Strategy and Action Plan (2024–2030). Retrieved 24 July 2025 from https://iklim.gov.tr/db/turkce/icerikler/files/CLIMATE%20CHANGE%20MITIGATION%20STRATEGY%20AND%20ACTION%20PLAN%20_EN(1).pdf.

Tian, P., Li, J., Cao, L., et al. (2021). Assessing spatiotemporal characteristics of urban heat islands from the perspective of an urban expansion and green infrastructure. *Sustainable Cities and Society*. https://doi.org/10.1016/j.scs.2021.103208

Tsou, J., Zhuang, J., Li, Y., & Zhang, Y. (2017). Urban heat island assessment using the Landsat 8 data: A case study in Shenzhen and Hong Kong. *Urban Science, 1*, Article 1010010. https://doi.org/10.3390/urbansci1010010

TUIK (2025) Turkish Statistical Institute, Address-Based Population Registration System 2024 Results https://data.tuik.gov.tr/Bulten/Index?p=Adrese-Dayali-Nufus-Kayit-Sistemi-Sonuclari-2024-53783#:~:text=%C4%B0stanbul'un%20n%C3%BCfusu%2C%20bir%20%C3%B6nceki,103%20ki%C5%9Fi%20ile%20Antalya%20izledi.

Villanueva-Solis, J. (2017). Urban heat island mitigation and urban planning: The case of the Mexicali, B. C. Mexico. *American Journal of Climate Change*. https://doi.org/10.4236/ajcc.2017.61002

Wang, J., & Ouyang, W. (2017). Attenuating the surface urban heat island within the local thermal zones through land surface modification. *Journal of Environmental Management*. https://doi.org/10.1016/j.jenvman.2016.11.059

Wang, R., Wang, M., Zhang, Z., Hu, T., Xing, J., He, Z., & Liu, X. (2022). Geographical detection of urban thermal environment based on the Local Climate Zones: A case study in Wuhan, China. *Remote Sensing, 14*(5), Article 1067. https://doi.org/10.3390/rs14051067

Weng, Q., Fu, P., & Gao, F. (2014). Generating daily land surface temperature at Landsat resolution by fusing Landsat and MODIS data. *Remote Sensing of Environment*. https://doi.org/10.1016/j.rse.2014.02.003

Worldbank data (2025) Urban Population (% of Population) Turkey. Retrieved 28 July 2025 from https://data.worldbank.org/indicator/SP.URB.TOTL.IN.ZS?locations=TR

Wu, J., Liu, C., & Wang, H. (2022). Analysis of spatio-temporal patterns and related factors of thermal comfort in subtropical coastal cities based on local climate zones. *Building and Environment, 207*, Article 108568. https://doi.org/10.1016/j.buildenv.2021.108568

Wu, Y., Liu, Y., Li, M., Hong, W., & Wang, C. (2025). Investigating and optimizing the impact of urban landscape patterns on heat island spatial distribution at the local climate zone scale. *SSRN*. https://doi.org/10.2139/ssrn.5336523

Yang, J., Wang, Y., Xiu, C., et al. (2020). Optimizing local climate zones to mitigate urban heat island effect in human settlements. *Journal of Cleaner Production*. https://doi.org/10.1016/j.jclepro.2020.123767

Yilmaz, D., & Ozturk, S. (2024). Urban heat island from a 3D modeling perspective—A review. *Environmental Modeling & Assessment*. https://doi.org/10.1007/s10666-024-09986-6

Zhang, H., Qi, Z., Ye, X., et al. (2013). Analysis of land use/land cover change, population shift, and their effects on spatiotemporal patterns of urban heat islands in metropolitan Shanghai, China. *Applied Geography*. https://doi.org/10.1016/j.apgeog.2013.07.021

Zhang, X., Estoque, R. C., Murayama, Y., & Ranagalage, M. (2021a). Capturing urban heat island formation in a subtropical city of China based on Landsat images: Implications for sustainable urban development. *Environmental Monitoring and Assessment*. https://doi.org/10.1007/s10661-021-08890-w

Zhang, Y., Li, D., Liu, L., Liang, Z., Shen, J., Wei, F., & Li, S. (2021b). Spatiotemporal characteristics of the surface urban heat island and its driving factors based on local climate zones and population in Beijing, China. *Atmosphere, 12*(10), Article 1271. https://doi.org/10.3390/atmos12101271

Zhao, C., Jensen, J., Weng, Q., et al. (2019). Application of airborne remote sensing data on mapping local climate zones: Cases of three metropolitan areas of Texas, U.S. *Computers, Environment and Urban Systems, 74*, 175–193. https://doi.org/10.1016/j.compenvurbsys.2018.11.002

Zhao, L., Lee, X., Smith, R. B., & Oleson, K. (2014). Strong contributions of local background climate to urban heat islands. *Nature*. https://doi.org/10.1038/nature13462

Zhao, M., Cai, H., Qiao, Z., & Xu, X. (2016). Influence of urban expansion on the urban heat island effect in Shanghai. *International Journal of Geographical Information Science*. https://doi.org/10.1080/13658816.2016.1178389

Zhao, Z., Sharifi, A., Dong, X., et al. (2021). Spatial variability and temporal heterogeneity of surface urban heat island patterns and the suitability of local climate zones for land surface temperature characterization. *Remote Sensing*. https://doi.org/10.3390/rs13214338

Zhou, X., & Chen, H. (2018). Impact of urbanization-related land use land cover changes and urban morphology changes on the urban heat island phenomenon. *Science of the Total Environment*. https://doi.org/10.1016/j.scitotenv.2018.04.091

Publisher's Note

Springer Nature remains neutral with regard to jurisdictional claims in published maps and institutional affiliations.